# Effect of cooling rate after solution treatment on subsequent phase separation during aging of Fe-Cr alloys: a small-angle neutron scattering study

Xin Xu[1, *], Joakim Odqvist[1], Magnus Hörnqvist Colliander[2], Stephen King[3], Mattias Thuvander[2], Axel Steuwer[4, 5], Peter Hedström[1]

[1]Dept. Materials Science and Engineering, KTH Royal Institute of Technology, Stockholm, SE-100 44, Sweden

[2]Dept. Physics, Chalmers University of Technology, Göteborg, SE-412 96, Sweden

[3]ISIS Facility, Rutherford Appleton Laboratory, Didcot, OX11 0QX, United Kingdom

[4]University of Malta, Msida, MSD 2080, Malta

[5]Nelson Mandela Metropolitan University, Gardham Avenue, Port Elizabeth 6031, South Africa

*Corresponding author: xinx@kth.se

## Abstract

The effect of cooling rate after solution treatment on the initial structure of concentrated binary Fe-Cr alloys and the effect of the initial structure on phase separation during subsequent aging has been investigated. The nano-scale compositional fluctuations in the bulk of the alloys are studied using small-angle neutron scattering and the results are compared with simulations using the Cahn-Hilliard-Cook (CHC) model. The alloys investigated represent different mechanisms of phase separation and at higher Cr content, when spinodal decomposition (SD) is favored, the initial Cr compositional fluctuations due to slow cooling after solution treatment reduce the kinetics of phase decomposition, whereas, at lower Cr composition when nucleation and growth is favored, the kinetics of phase decomposition is more rapid. Regardless of the nominal Cr composition of the alloy, the phase decomposition after extended aging up to 300 h at 748 K is always larger for the more non-random initial structure. The CHC modeling of the cooling process and subsequent initial aging (below 10 h) is in reasonable qualitative agreement with the experimental results for the Fe-40 wt.% Cr alloy decomposing via SD. However, the modeling approach must be refined for accurate quantitative modeling of the full SD process, including coarsening.

**Key words**: Phase separation, spinodal decomposition, cooling rate, small-angle neutron scattering, stainless steel

## 1. Introduction

The body-centered cubic (bcc) and tetragonal (bct) phases in Fe-Cr based alloys, i.e. stainless steels, will experience phase separation (PS) when they are heat treated within the miscibility gap. Hence, the assumed initially random alloy decomposes into Fe-rich (α) and Cr-rich (α') regions, causing the so-called "475 °C embrittlement" with increased hardness and decreased toughness of the alloy. Since these materials are promising candidates in e.g., future designs of nuclear power plants [1,2], structural integrity is clearly important and the "475 °C embrittlement" must be avoided. Currently there are significant research efforts on-going to study the mechanisms controlling the phase decomposition under different conditions, and to find ways of mitigating the embrittlement.

It is known that the bcc/bct phase in solution treated Fe-Cr alloys is not always a random alloy. Instead, compositional fluctuations of Cr may occur already during the solution treatment and depends on the solution treatment temperature as well as the cooling rate after solution treatment [3–11]. Huston et al. [3] simulated spinodal decomposition (SD) during continuous cooling, using the linearized Cahn-Hilliard model. They suggested a critical cooling rate and that by exceeding the critical cooling rate SD will be avoided, but if the cooling rate is slower than the critical rate, decomposition will occur. In their simulations, slower cooling rates led to more pronounced decomposition. Carmesin et al. [4] further studied SD during continuous cooling by performing simulations using: the linearized Cahn-Hilliard model specifically incorporating thermal fluctuations, i.e. the Cook extension, the non-linear Langer-Bar-on-Miller theory (LBM), and the Monte Carlo technique. Their results indicated that PS evolves faster for samples cooled with finite rates rather than in an instantaneous process. Later experimental work have also confirmed that PS can occur in the ferrite during cooling from the solution treatment temperature in both ferritic and duplex stainless steels [5,6]. The hardness of ferrite in unaged duplex stainless steels was evaluated to be greater for samples cooled with lower rates and this was attributed to more severe PS at lower cooling rates [12]. Atom probe tomography measurements verified that the amplitude of Cr compositional fluctuations was larger for unaged samples that were cooled at slower rates, and that this initial difference was also present after aging [13]. As mentioned, it is also known that the solution treatment temperature affects the initial structure. Vintaykin et al. [7] and LaSalle and Schwartz [8] have shown that solution treatments of Fe-Cr alloys at different temperatures above the miscibility gap lead to different small-angle neutron scattering (SANS) results, indicating different microstructures. Moreover, the kinetics of SD was found to depend on this initial microstructure, and a higher solution treatment temperature resulted in slower kinetics of SD. Mirebeau et al. [14,15] studied the short range order of Fe-Cr alloys thermally treated at 703 K by diffuse neutron scattering [16]. They showed that Fe-Cr is prone to ordering when the Cr content is below 0.107, while clustering occurs when the Cr content is above 0.107. Theoretical calculations predicted a similar tendency for the short-range order (SRO) parameter with a change of sign with increasing Cr content [17–21]. The tendency of Cr clustering in Fe-Cr alloys with higher Cr contents has also been shown by Zhou et al. [10,11,22].

As portrayed in the literature survey above, the initial structure is an important factor when it comes to predicting the evolution of PS during aging. The cooling rate after solution treatment seems to affect the initial structure and it is therefore important to have a greater understanding of the effect of cooling rates, and also its alloying dependence in continuous cooling experiments. Furthermore, studying the aging behavior of samples cooled in different ways might improve our understanding of the effect of the initial structure on PS. Thus, in the present work we conducted a systematic investigation of the effect of cooling rate after solution treatment on the initial structure of Fe-Cr alloys and, furthermore, the effect of the initial structure on PS during subsequent aging. The initial structure after solution treatment and the kinetics of PS are investigated using small-angle neutron scattering (SANS). SANS theories consider the structure factor which can be directly linked to Cahn-Hilliard (CH) model. Therefore, the experimental results are compared to simulations using the linearized Cahn-Hilliard-Cook (CHC) model.

## 2. Methodology

Binary Fe-Cr alloys with chemical compositions listed in Table 1 were prepared by vacuum arc melting. Fe-20Cr and Fe-40Cr alloys were cut into around 10×10×1.7 $mm^3$ samples, whereas Fe-25Cr and Fe-35Cr alloys were cut into around 5×5×1.7 $mm^3$ samples. Thereafter, all samples were solution treated at 1373 K for 2 h in a slight overpressure of pure argon. The cooling after

solution treatment was performed in two ways: i) furnace cooling (FC) or ii) quenching in brine (BQ). The entire cooling process from solution treatment temperature to room temperature for FC samples was $t_{FC}$=5.5 h and the cooling through the temperature interval where the PS kinetics is reasonably fast, i.e. 573-853 K [23] was 73 min giving an average cooling rate of ~ 4 K/min (the cooling rate is 5.7 K/min at 853 K and 3 K/min at 573 K). Both FC and BQ samples were then aged at 748 K for up to 300 h as detailed in Table 1. The thermal cycles are also schematically shown in Fig. 1. For simplicity, the sample notation from hereon is: cooling method, alloy composition and aging time. For example, FC20Cr1 represents alloy Fe-20Cr cooled by FC and aged at 748 K for 1 h. The unaged samples are represented by zero aging time.

**Table 1.** Chemical compositions of Fe-Cr alloys (wt.%) and the isothermal aging times at 748 K. FC and BQ represent furnace cooling and quenching in brine, respectively.

| Alloy | Cr | C | Si | Mn | S | P | N | Ni | Fe | Cooling process | Aging time (h) |
|---|---|---|---|---|---|---|---|---|---|---|---|
| 20Cr | 19.8 | 0.002 | 0.03 | 0.11 | 0.004 | 0.005 | 0.008 | -- | Bal. | FC | 0, 1, 10, 300 |
| | | | | | | | | | | BQ | 0, 1, 10, 300 |
| 25Cr | 25.28 | 0.002 | 0.09 | 0.005 | 0.006 | 0.004 | 0.009 | 0.03 | Bal. | FC | 0, 300 |
| | | | | | | | | | | BQ | 0, 300 |
| 35Cr | 36.10 | 0.005 | 0.09 | 0.006 | 0.005 | 0.005 | 0.008 | 0.02 | Bal. | FC | 0, 300 |
| | | | | | | | | | | BQ | 0, 300 |
| 40Cr | 41.09 | 0.007 | 0.105 | 0.114 | 0.006 | 0.006 | 0.006 | 0.02 | Bal. | FC | 0, 1, 10, 300 |
| | | | | | | | | | | BQ | 0, 1, 10, 300 |

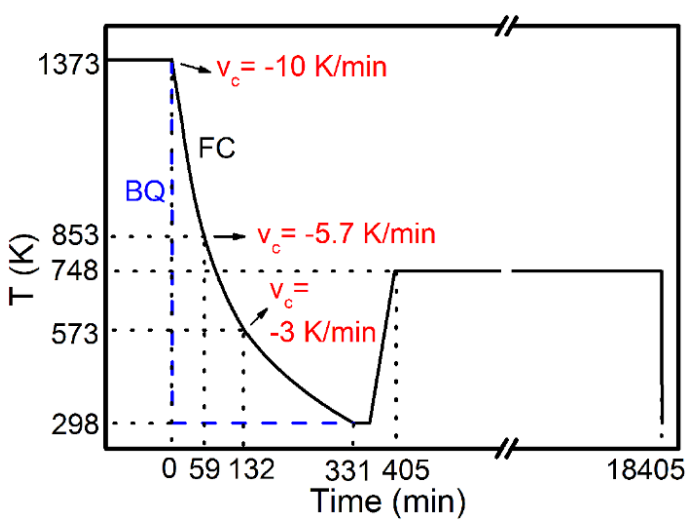


Fig. 1 Schematic diagram of the heat treatment cycles imposed on the different samples ($v_C$ is the cooling rate).

The samples were ground and polished by sand papers (up to P1200 grit) to 1.5 mm thickness in order to remove the oxide layer prior to the neutron experiments. The LOQ diffractometer at the ISIS Pulsed Neutron Source (Oxfordshire, UK) was used for SANS measurements. This instrument uses the time-of-flight technique, coupled with a broad range of incident neutron wavelengths and two position-sensitive detectors, a multi-wire proportional gas counter and an annular scintillator area detector [24], to provide a simultaneous scattering vector range of 0.008

$\leq Q \leq 1.4$ Å$^{-1}$ (where $Q = 4\pi\sin\theta/\lambda$, $2\theta$ is the scattering angle, and $\lambda$ is the wavelength). The neutron beam was collimated to a diameter of 4 mm and data were collected for 2 h per sample at room temperature. The raw SANS data were corrected for the efficiency and spatial linearity of the detectors, instrumental background, sample transmission and illuminated volume using the Mantid framework (version 3.2.1) [25,26], to yield the macroscopic coherent differential scattering cross section ($\partial\Sigma(Q)/\partial\Omega$) as a function of Q. This was then placed onto an absolute scale using the scattering from a standard sample (a partially-deuterated polymer blend of known molecular weight) [27]. $\partial\Sigma(Q)/\partial\Omega$, colloquially called the intensity, $I(Q)$, is directly related to both the nuclear and magnetic nanostructure of the alloys. But in this study, the nuclear and magnetic scattering were not separated (using a saturating magnetic field) since the prior reports [8,28–30] have claimed that the nuclear and magnetic scattering have a similar $Q$-dependence at $Q$>0.05 Å$^{-1}$ for the early stage of phase separation. The magnetic scattering from magnetic domains mainly contributes to $I(Q)$ at low-$Q$ ($Q$<0.05 Å$^{-1}$), and it will not interfere with the length-scale of interest in this study, i.e. the length-scale of Cr fluctuations, when $I(Q)$ is averaged over all directions [8,28–30].

In the two-phase model, where the second phase (precipitate) is embedded in the matrix, assuming the precipitates are identical and the concentration of the precipitates is high, $I(Q)$ can be generally expressed as [31–33]

$$I(Q) = N_P V_P^2 (\Delta\delta)^2 P(Q) S(Q) \quad (1)$$

where $N_P$ is the number density of precipitates, $V_P$ is the volume of a precipitate (such that $N_P V_P = \Phi_P$, the volume fraction), and $\Delta\delta = \rho_p - \rho_m$ is the difference in neutron scattering length density between the precipitate ($\rho_p$) and matrix ($\rho_m$). $(\Delta\delta)^2$ is called the scattering contrast which is critical to distinguish the precipitate from the matrix. It also indicates the composition difference between the precipitate and matrix since $\rho_p$ and $\rho_m$ are determined by the respective phase compositions [33]. $P(Q)$ is the single-particle form factor which depends on the shape and size of the considered precipitate domain [34]. $S(Q)$, the structure factor, is the Fourier transform of the static pair correlation function, which describes the correlation between precipitates. When the concentration of precipitates is low, $S(Q) \rightarrow 1$, meaning the inter-precipitate correlations can be neglected and the scattering is dominated by P(Q) [31,32]. However, when the concentration of precipitates is high, $S(Q)$ endows $I(Q)$ with an interference peak that becomes more pronounced as the correlations become more definitive. The position ($Q_P$) of this interference peak represents an average characteristic length scale ($d$), through $d = 2\pi/Q_P$ [33]. In this study, Fe-20Cr decomposes via a non-classical nucleation and growth (NG) mechanism to give a structure consisting of $\alpha'$ particles and $\alpha$ matrix, $d$ is the average distance between $\alpha'$ domains [23,35]. Fe-25Cr is in the transition region between NG and SD and, hence, a structure with both particle and interconnected features could be present [23,36,37]. The alloy composition is in the NG region according to available thermodynamic descriptions (at 748 K, the spinodal limit in the Fe-rich side is at 29.7 at.% [37] and 35.7 at.% [38]). It is therefore believed that the Fe-25Cr alloy mainly decompose via NG. On the other hand, Fe-35Cr and Fe-40Cr mainly decompose via SD leading to an interconnected structure [37]. In these alloys $d$ is the average wavelength characterizing the spinodal structure. The above description also implies that the peak intensity ($I_P$) is an indicator of the evolution of the nanostructures as has been previously shown [30,39,40]. $Q_P$ and $I_P$ were determined from the SANS patterns as described by Xu et al. [40] using the similar method as in [30]. To accomplish this, the scattering due to PS was isolated by subtracting the background signal as shown in Fig. 2. In this study, the $I(Q)$ of BQ unaged samples was treated as that of homogeneous samples without decomposition due to Q-independent scattering beyond $Q$=0.1 Å$^{-1}$. As shown in Fig. 2a, the SANS of BQ unaged samples

can be fitted by a power law function. Therefore, the background of different conditions were fitted in the same way, namely, by a power law function of the form, $I_b=x+yQ^z$, see Fig. 2b. Then $I(Q)$ was normalized by $I_b$ such that, $I_n=I(Q)/I_b$ and the plot of $I_n$ *vs*. log $Q$ was fitted by a Gaussian function, $I_G$ (Fig. 2c). Finally, the scattering function for PS, $I_{PS}$, was separated as $I_{PS}=I_b(I_G-1)$ (Fig. 2d). Since $I_G \geq 1$, these procedures ensure that all the data have positive intensities after subtracting the background.

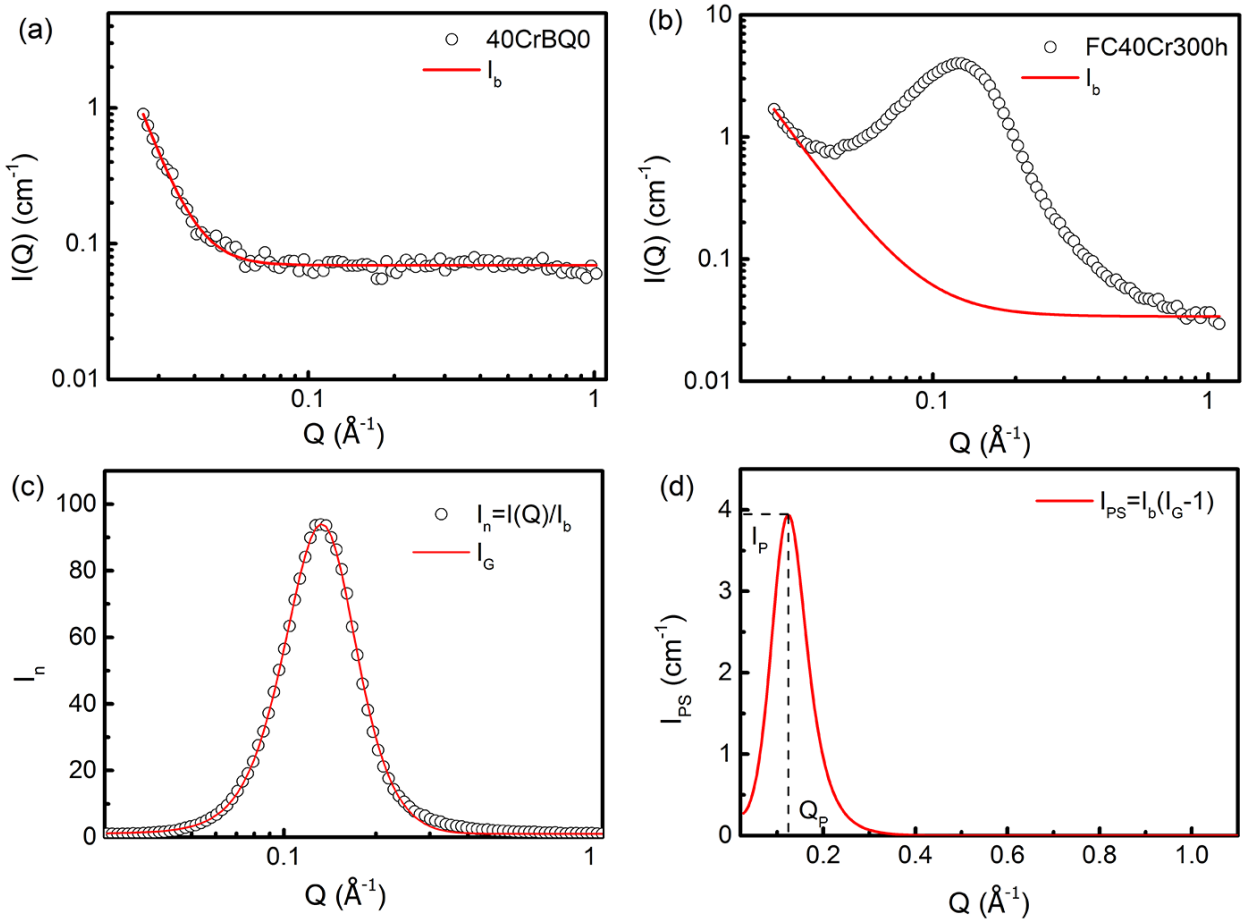


Fig. 2 Schematic of fitting the scattering functions and quantifying the PS: (a) fitting of data of BQ unaged samples; (b) fitting of background, $I_b$, by a power law function of the form, $I_b=x+yQ^z$, (c) fitting of the normalized signal, $I_n=I(Q)/I_b$, by a Gaussian function, $I_G$; (d) the scattering function for phase separation, $I_{PS}$, was separated as $I_{PS}=I_b(I_G-1)$. $Q_P$ and $I_P$ are the peak position and peak intensity.

The PS during cooling and subsequent isothermal aging at 748 K was simulated for BQ40Cr and FC40Cr alloys using the CHC model. The structure factor $S(Q,t)$ in the CHC framework can be written as [8,41]:

$$S(Q,t)=\frac{RT}{f''+2\kappa Q^2}+\left[S_0-\frac{RT}{f''+2\kappa Q^2}\right]\times\exp\left\{-2M(f''+2\kappa Q^2)Q^2t\right\} \quad (2)$$

where $S_0=S(Q,t=0)$ is the initial structure factor, $f''$ is the second derivative of the molar Gibbs energy with respect to the mole fraction of Cr taken from the Thermo-Calc Software TCFE8 Steels/Fe-alloys database version 8 (the binodal solubility limits at 748 K are at 15.7 and 88.3 at.% Cr, and $f''$ is $-7.35\times10^3$ J/mol at 748 K) [42], $\kappa$ is the gradient energy coefficient: $\kappa=a^2L^0_{CrFe}/2$, $a$ is the interaction distance taken to be 2.5 Å and $L^0_{CrFe}$ is the regular solution

parameter: $L^0_{CrFe}$=20500-9.68$T$ [38]. $R$ and $T$ are the gas constant and absolute temperature, respectively. $M$ is the atomic mobility: $M=x_0(1-x_0)[x_0M_{Fe}+(1-x_0)M_{Cr}]$, where $x_0$ is the average molar content of Cr, and $M_{Fe}$ and $M_{Cr}$ are the atomic mobilities for Cr and Fe, respectively. The atomic mobilities were taken from the Thermo-Calc Software MOBFE2 Steels/Fe-alloys database version 2 [43]. For the BQ condition $S_0$=1, assuming that no PS takes place during the quenching. On the other hand, for the FC condition a function ($T = 1377\text{-}13.19t + 8.64\times10^{-2}t^2\text{-}3.29\times10^{-4}t^3 + 6.46\times10^{-7}t^4\text{-}5.10\times10^{-10}t^5$, where T is temperature, $t$ is time) was fitted to the experimental cooling curve in Fig. 1. This cooling cycle was then used to calculate the structure factor according to eq. (2) after discretizing the cooling cycle in discrete temperature steps. A similar procedure was suggested by Carmesin et al. [4]. The furnace cooling started at 1377 K and ended at room temperature. For each new temperature step the structure factor $S$ calculated in the prior step was set to $S_0$. In this way the effect of a finite cooling rate on the PS could be simulated. The final structure factor at room temperature was then used as $S_0$ in eq. (2) for the isothermal aging at 748 K assuming that the heating from room temperature to the aging temperature was so rapid that no additional PS could take place.

## 3. Results

Fig.3 shows the SANS data of Fe-Cr alloys subjected to different cooling rates after solution treatment, and then aging for different times at 748 K. As can be seen in Fig. 3a, the data of unaged samples from the same alloys are significantly different when comparing the two different conditions BQ and FC. After a steady decrease in intensity in the low-$Q$ range, the SANS data of the BQ samples level off beyond $Q$=0.1 Å$^{-1}$, i.e. no nano-scale structure is evident. However, the FC unaged samples do show a nano-scale structure with a broad correlation peak appearing in the scattering data. All scattering data of the aged samples have this type of shape and it should be interpreted as PS in both unaged FC and aged samples. The slight convex curvature of the scattering data at low-$Q$ is most likely due to some oxide inclusions that were identified using scanning electron microscopy, but since the length-scale is not interfering with the PS it is simply neglected from hereon as well as in the background fitting.

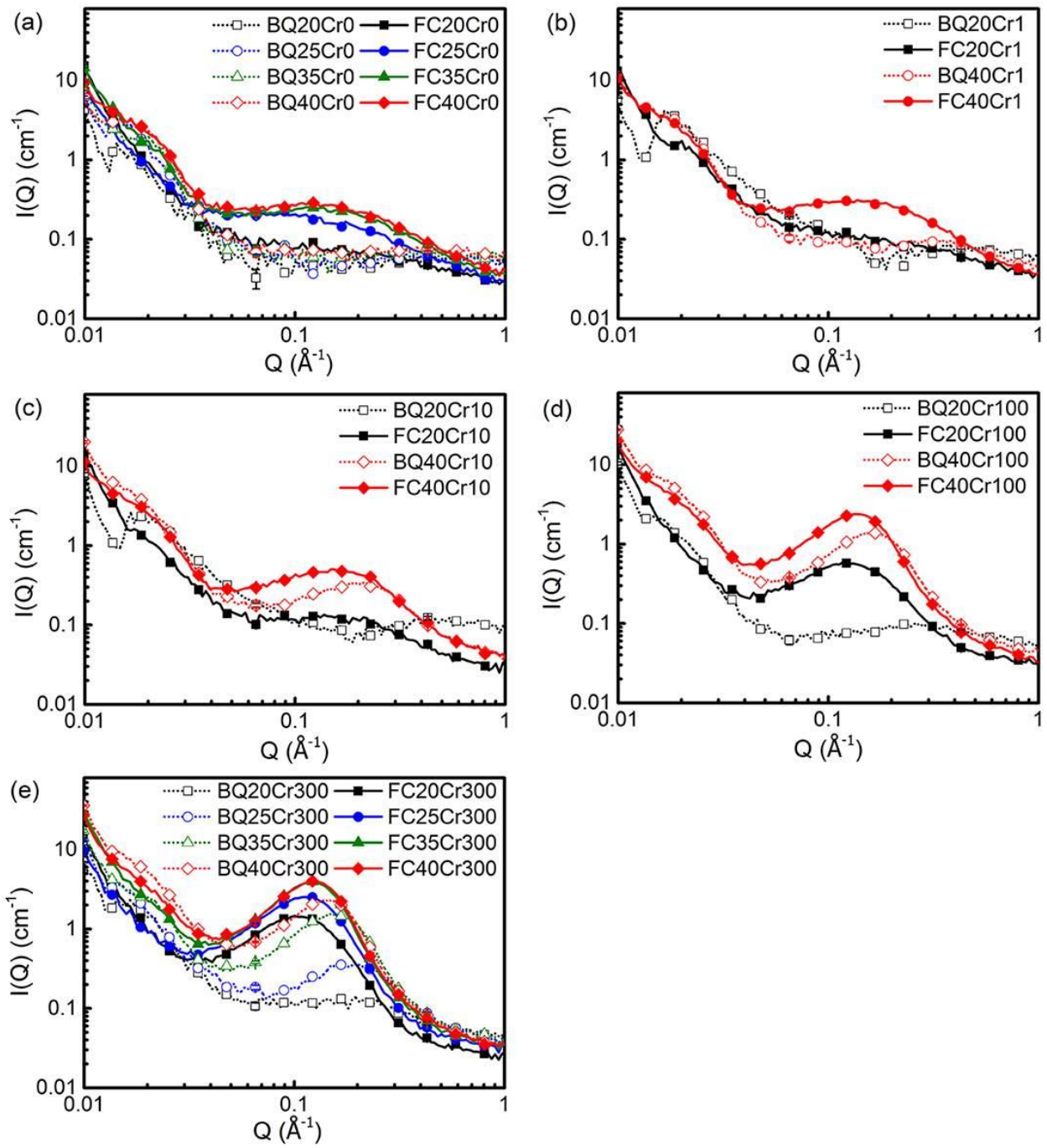


Fig. 3 SANS data of Fe-Cr cooled at different rates: (a) unaged, (b) 1 h aging, (c) 10 h aging, (d) 100 h aging and (e) 300 h aging. Note that the error bar is quite small and covered by the symbols.

The quantification of $d$ and $I_P$ for the different conditions is tabulated in Table 2 and it can be seen that FC unaged samples have relatively large $I_P$, which means that the samples have decomposed, and the $d$ values show the length-scale of the decomposition. The values of $d$ and $I_P$ for FC unaged samples are comparable to, or even larger than, those of BQ samples aged for 10 h from the same alloys, though the entire FC process time is shorter than 10 h. These results indicate that the size of $\alpha'$ and the compositional fluctuations in the unaged FC samples are already quite well developed.

Table 2 Characteristic distance, $d$, and peak intensity, $I_P$, of different alloy compositions and aging conditions.

| Alloy conditions | $d$ (Å) | $I_P$ (cm$^{-1}$) | Alloy conditions | $d$ (Å) | $I_P$ (cm$^{-1}$) |
|---|---|---|---|---|---|
| BQ20Cr1 | 13.8±0.4 | 0.04±0.007 | BQ35Cr300 | 40.6±0.2 | 1.50±0.34 |
| BQ20Cr10 | 13.9±0.6 | 0.05±0.009 | FC35Cr0 | 44.0±0.3 | 0.21±0.02 |
| BQ20Cr100 | 26.3±0.4 | 0.05±0.005 | FC35Cr300 | 51.8±0.1 | 3.87±0.53 |
| BQ20Cr300 | 31.6±0.5 | 0.09±0.01 | BQ40Cr1 | 19.4±0.4 | 0.06±0.005 |
| FC20Cr0 | 30.9±0.8 | 0.03±0.007 | BQ40Cr10 | 32.2±0.3 | 0.31±0.02 |
| FC20Cr1 | 37.2±0.4 | 0.07±0.01 | BQ40Cr100 | 39.4±0.2 | 1.36±0.03 |
| FC20Cr10 | 42.0±0.4 | 0.10±0.01 | BQ40Cr300 | 44.0±0.1 | 2.27±0.26 |
| FC20Cr100 | 50.7±0.2 | 0.55±0.03 | FC40Cr0 | 43.1±0.3 | 0.23±0.02 |
| FC20Cr300 | 59.5±0.1 | 1.43±0.06 | FC40Cr1 | 44.2±0.3 | 0.28±0.02 |
| BQ25Cr300 | 33.6±0.3 | 0.33±0.04 | FC40Cr10 | 43.7±0.5 | 0.47±0.04 |
| FC25Cr0 | 41.7±0.5 | 0.11±0.01 | FC40Cr100 | 46.2±0.1 | 2.37±0.20 |
| FC25Cr300 | 55.3±0.1 | 2.51±0.25 | FC40Cr300 | 50.6±0.1 | 3.94±0.62 |

For aged samples, the peak in the SANS data for FC samples is more pronounced than for the BQ samples for the same alloy, exposed to the same aging treatment (Fig. 3 and Table 2). The values of $d$ and $I_P$ of FC samples are larger than those of BQ samples. This indicates that samples with slower cooling rates have larger characteristic distances and composition amplitudes and/or volume fraction of the precipitate. It should be noted that the difference caused by the applied cooling process after solution treatment is still large after 300 h aging, though the FC process time is rather short in comparison with the aging time of 300 h. For the same thermal treatment, alloys with higher Cr content generally have larger $d$, and $I_P$ with the exception for $d$ of the FC samples that have been aged for 300 h. These samples have rather similar $d$.

Theoretical models have illustrated that the evolution of $Q_P$, and therefore $d$, and $I_P$ with aging time can be described by power laws, namely, $Q_P \propto t^{-a}$, $d \propto t^{a}$, and $I_P \propto t^{b}$ [44–46]. As shown in Fig. 4a and b, $a$ for BQ 20Cr and 40Cr is 0.16 and 0.10, and for FC20Cr and FC40Cr it is 0.10 and 0.03, respectively. $d$ of FC40Cr does not change much within the aging period, while $d$ of other conditions has an obvious increase. $b$ for BQ20Cr and BQ40Cr is 0.12 and 0.66, and for FC20Cr and FC40Cr it is 0.64 and 0.46, respectively. Hence, the kinetics of PS during aging is slower for FC40Cr than for BQ40Cr according to both $a$ and $b$. This is consistent with the results of the Monte Carlo simulations by Hyde et al. [47]. They found that slower cooling rates result in smaller $a$ during aging for a simple A-B alloy with cubic lattice. The above $a$ values also indicate that the decomposition is still in the early stage and that they have not reached the coarsening stage where $d \propto t^{1/3}$ as shown in [36] based on the theories of Lifshitz-Slyozov-Wagner [48,49]

and Huse [50]. On the other hand, for Fe-20Cr, $d$ of the FC samples increases slower with aging time compared to that of the BQ samples, whereas, $I_P$ shows the opposite trend. $d$ and $I_P$ of FC20Cr and BQ20Cr are significantly different after 300 h aging. By contrast, $d$ and $I_P$ of FC40Cr and BQ40Cr almost converge after 300 h aging. The differences between values for BQ35Cr and FC35Cr are also smaller than that of Fe-25Cr, see Fig. 4 and Table 2. Though the effect of the cooling rate should eventually be eliminated for all alloys, the differences fade faster during aging for alloys with higher Cr content.

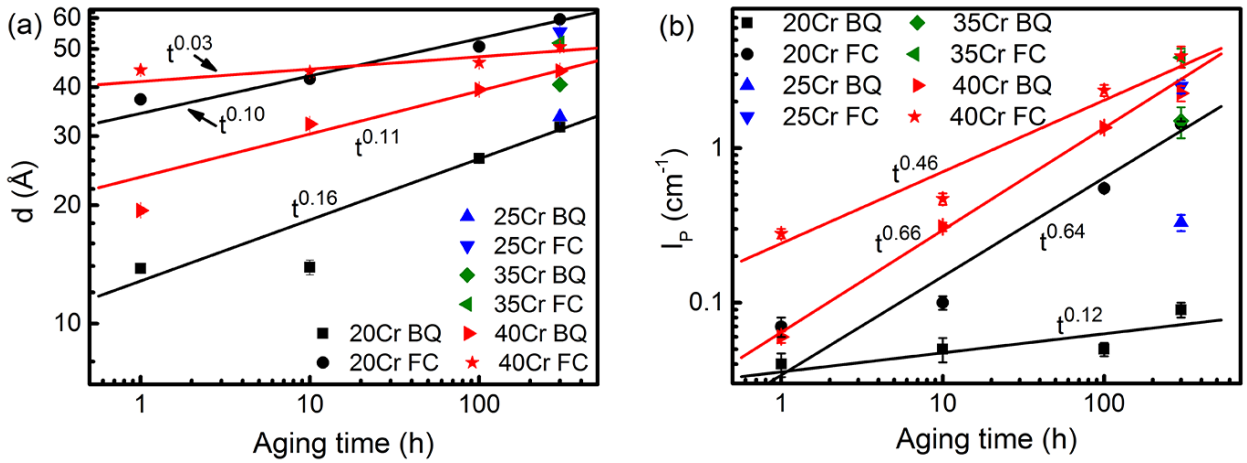


Fig. 4 Values of (a) $d$ and (b) $I_P$. The values of Fe-20Cr and Fe-40Cr alloys are fitted by power laws using the linear regression approach. The linear regression coefficient $R^2$ for the fitting of $d$ is: $R^2$(20Cr BQ)=0.86, $R^2$(20Cr FC)=0.91, $R^2$(40Cr BQ)=0.65, $R^2$(40Cr FC)=0.99, and for the fitting of $I_P$ is: $R^2$(20Cr BQ)=0.93, $R^2$(20Cr FC)=0.99, $R^2$(40Cr BQ)=0.93, $R^2$(40Cr FC)=0.94.

The simulated structure factor at 748 K aging for the BQ condition can be seen in Fig. 5a and d. Here the atomic mobility $M$ in eq. (2) was adjusted to $3.1\times10^{-27}$ m$^2$mol/Js so the characteristic distance d for $t$=1 h between the experiments ($d$=19.4 Å from Table 2) and simulations ($d$=19.8 Å) was as close as possible. This mobility was then used for the remaining simulations of aging at 748 K for the BQ and FC conditions. The simulated time was restricted to $t$=10 h since longer times resulted in an unrealistically large structure factor. This is not surprising since the linearized CHC should be valid only for early stages of PS. Comparing the characteristic distance from experiments for BQ40Cr10 ($d$=32.2 Å) and simulations ($d$=27.8 Å), the agreement is considered to be reasonable.

The simulated structure factors during FC can be seen in Fig. 5b. Outside the miscibility gap [38], the structure factor changes only slightly but once inside the miscibility gap and inside the spinodal, a clear peak in the structure factors develops, i.e. PS occurs during cooling, and it has a distinct characteristic distance, see Fig. 5b. As the temperature is decreased, d becomes smaller and the peak intensity, $S(Q_P,t)$, becomes larger. This is consistent with the results from Carmesin et al. [4]. When the temperature is lowered below about 700 K, $d$ and $S(Q_P,t)$ remain almost the same.

The effect of a finite cooling rate on the microstructure evolution during aging at 748 K is clearly seen in Fig. 5c and d, where the characteristic distance starts from a much higher value compared to the BQ condition. Although the absolute values of $d$ are not in perfect agreement with experiments the trend is qualitatively captured by the CHC model. From Fig. 5d, it can be seen that $d$ of FC is almost unchanged with aging time, while $d$ of BQ increases with aging time. In addition, the coherent differential cross section, $I(Q)_{CHC}$, derived from $S(Q,t)$ is presented

together with the experimental results in Fig. 5e and f. The maximum value, $I(Q_P)_{CHC}$, of $I(Q)_{CHC}$, is also shown for comparison with experimental values in Fig. 5d. $I(Q)_{CHC}$ is calculated in the same way as in [8,9]:

$$I(Q)_{CHC} = N_v x_{Cr}(1-x_{Cr})(b_{Cr}-b_{Fe})^2 S(Q,t) \qquad (3)$$

where $N_v$=8.427×10$^{22}$ cm$^{-3}$ is the atomic number density of Fe-40Cr, $x_{Cr}$=42.76 at. % is the atomic fraction of Cr, $b_{Cr}$=3.635×10$^{-13}$ cm, $b_{Fe}$=9.45×10$^{-13}$ cm [51] are the scattering length of Cr and Fe, respectively. $I(Q)_{CHC}$ corresponds to the nuclear scattering. LaSalle and Schwartz [8] reported that the nuclear and magnetic scattering of Fe-Cr have the identical Q dependence at the early stage of SD and the ratio of the nuclear scattering intensity to the total intensity is around 0.55 for Fe-32%Cr [28]. Therefore, $I_{PS}$ from SANS is multiplied by 0.55 and shown as $I_{SANS}$ in Fig. 5e and f, and the maximum value of $I_{SANS}$ is shown as $I(Q_P)_{SANS}$ in Fig. 5d. $I(Q_P)_{CHC}$ and $I(Q_P)_{SANS}$ both show the trend that the difference in the initial structure fade during aging, but the absolute values are somewhat different and, also, $I(Q_P)_{CHC}$ implies faster kinetics. The agreement between $I_{CHC}$ and $I_{SANS}$ is lower after 10 h aging as compared to 1 h aging, see Fig. 5e and f. The modelling results indicate that the kinetics of PS is faster for the BQ conditions than for the FC conditions, which is in good agreement with the SANS results. It should be pointed out that the excellent fitting of the SANS data by the CHC model in [8,9] is due to that $f''$, $M$ and $\kappa$ were used as fitting parameters, varying for each aging condition, instead of taking physically assessed quantities.

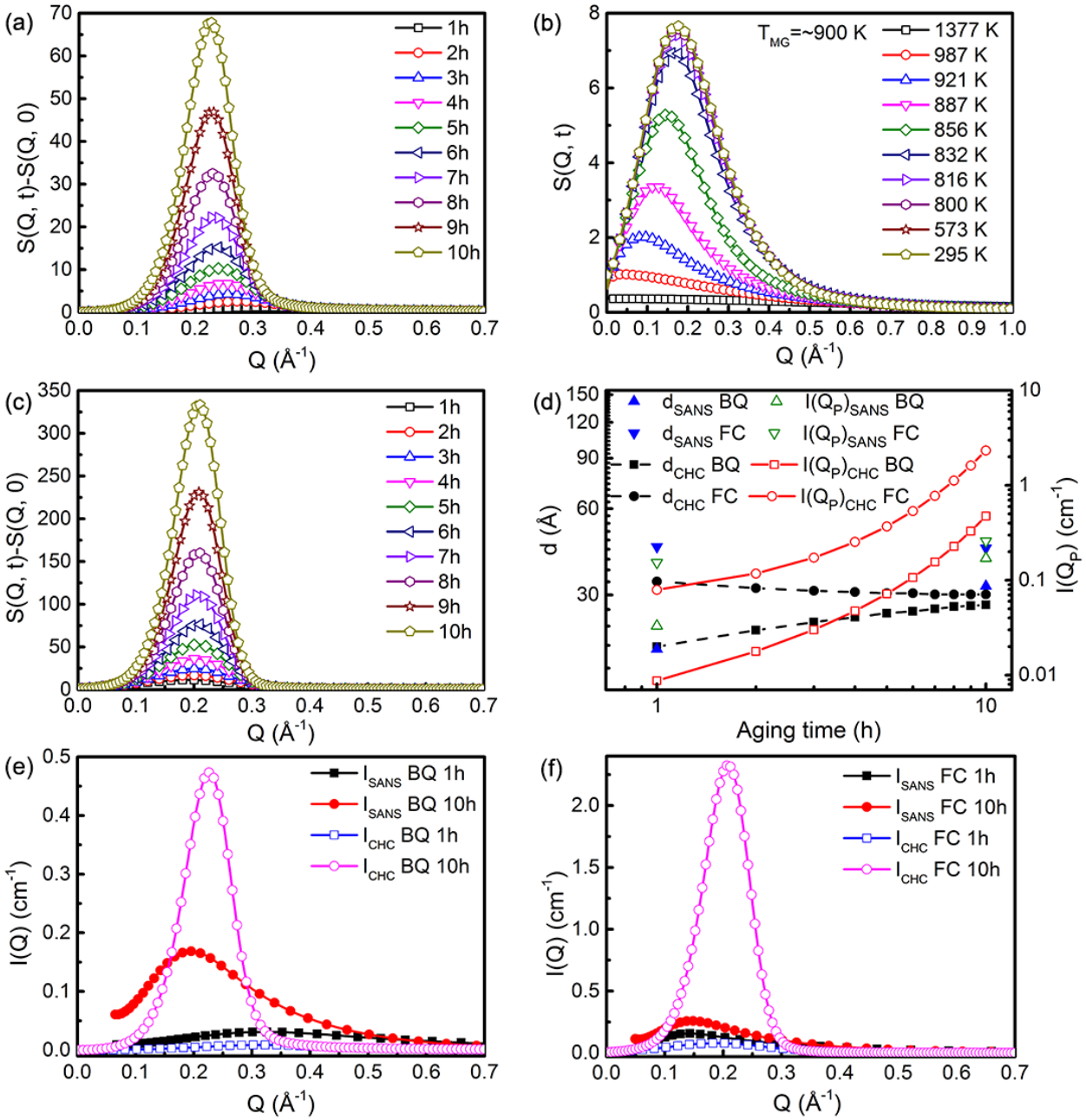


Fig. 5 Evolution of the structure factor, $S(Q,t)$, of Fe-40Cr simulated by the linearized CHC model: (a) BQ from 1377 K to room temperature followed by aging at 748 K for different times, (b) FC from 1377 K to room temperature (the temperature of the miscibility gap, $T_{MG}$=~900 K [38]), (c) aging of FC at 748 K for different times, (d) comparison of the evolution of d and $I(Q_P)$ during aging between CHC modeling and SANS, the intensity from SANS, $I_{SANS}$, and linearized CHC model, $I_{CHC}$, for (e) BQ conditions and (f) FC conditions.

## 4. Discussion

The experimental results presented in the present work show the effect of different cooling rates on the subsequent PS during aging of binary Fe-Cr alloys with different compositions. It is clear that the effect of the cooling rate is composition dependent and that slow cooling, that could arise

when thicker gauge sections are cooled after manufacturing, will lead to PS during the cooling process. This difference in the initial structure will then affect the subsequent aging kinetics and it was found that the PS kinetics will be slower for slowly cooled samples when the nominal Cr composition is 40 wt.%, whereas it will be faster for samples with a nominal Cr composition of 20 wt.%. This difference in PS kinetics is most likely due to the difference in PS mechanisms for different Cr compositions. Alloys with a low Cr content (e.g. 20 wt.%) are believed to decompose via NG and during slow cooling the initial nuclei will form, and these will grow and coarsen during the isothermal aging at 748 K. The process at 748 K is then mainly diffusion-controlled and comparing with the BQ samples where nucleation, growth and coarsening of the particles is a concurrent process it is reasonable to suggest that the FC samples would experience more rapid PS kinetics.

On the other hand, in alloys with a high Cr content (e.g. 40 wt.% Cr), which are believed to decompose via SD, the slow cooling will lead to the development of sinusoidal waves of a longer dominant wavelength since it depends on the critical wavelength, which increases with increasing temperature. In contrast, the BQ samples will have a shorter dominant wavelength during the aging since the critical wavelength at 748 K is smaller. Since SD is diffusion-controlled it is reasonable to assume that the PS kinetics would be slower for the longer wavelength structure due to the longer diffusion distance, i.e. this is most likely why the PS is slower for the FC than for the BQ initial samples when the Cr content of the alloy is 40 wt.%.

Comparing the experimental results with the CHC modeling results for the Fe-40Cr alloy, it is found that the model predictions can qualitatively capture the difference of the initial structures between BQ and FC as well as its effect on the aging kinetics in the early stage of SD. The early stage of SD can here be identified as aging at 748 K for less than 10 h, since already at 10 h, the exponential evolution of the structure factor intensity is starting to shoot-off and will become unreasonable, and in poor agreement with the experimental results. It should be noted that in practice the interesting time frames at 748 K are in the order of 10 h. The mechanical properties of the alloys will already then be affected and it has been shown in e.g. [52,53] that the impact toughness of these types of model alloys may be very low after aging for 10 h at 748 K and 773 K, in that case. Though the trend was predicted by the modeling, $I_{CHC}$ has a much higher peak intensity than $I_{SANS}$ for the 10 h aging condition in Fig. 5e and f. This may be attributed to the linearization of the Cahn-Hilliard model, which includes the use of a constant $M$ and a constant $f''$. This is a rather crude assumption and will break down for long aging times. Here $M$ was derived for BQ40Cr1 and remained the same for other conditions in the simulations since there is a lack of an accurate description of the composition dependent $M$. Better descriptions of $M$ should be pursued, which was also pointed out by Nastar [54] in the comparison between CH and Self-Consistent Mean Field theories. Moreover, the driving force for SD should be different at different stages due to varying composition gradients. Hence, $f''$ should differ at different stages of SD too. However, this is hard to handle in the linearized CHC model. More realistic modeling predictions of a larger part of the PS process would be highly desirable. It should be possible to move in that direction by implementing the non-linearized Cahn-Hilliard model and considering composition dependent $M$ as well as changing $f''$. Moreover, it is necessary to look more in detail on $\kappa$, because this term is controlling the sharpness of the interfaces of the decomposing nano-structure.

It should, however, be emphasized that there are additional factors connected to the initial structure that will affect the PS aging kinetics. Cr clustering that arises due to the short-range order tendency above the miscibility gap [10,14,15,22,55–57] is one such factor and it cannot be fully handled within a continuum approach such as the Cahn-Hilliard model. This effect is likely to be a contributing factor to the deviation between $I_{CHC}$ and $I_{SANS}$ in Fig. 5f. However, it has

been found that, at present, this effect seems to be difficult to handle even with atomistic simulations [11]. Further work on the modeling of the effect of the initial structure on the PS kinetics is therefore necessary to find a viable modeling route.

## 5. Conclusions

In the present work it is found that the cooling process after solution treatment of Fe-Cr alloys has a significant effect on the structure, and further, this structure will significantly affect the phase separation (PS) evolution during subsequent aging at 748 K. The alloys investigated represent different mechanisms of PS and at higher Cr content, when spinodal decomposition (SD) is favored, the initial Cr compositional fluctuations due to slow cooling after solution treatment reduce the kinetics of phase decomposition, whereas, at lower Cr composition when nucleation and growth (NG) is favored, the kinetics of phase decomposition is more rapid. Regardless of the nominal Cr composition of the alloy, the phase decomposition after extended aging up to 300 h at 748 K is always larger for the more non-random initial structure. The Cahn-Hilliard-Cook modeling of the cooling process and subsequent initial aging (up to about 10 h) is in reasonable qualitative agreement with the experimental results for the Fe-40 wt.% Cr alloy decomposing via SD. However, the modeling approach must be refined to enable accurate quantitative continuum modeling of the full SD process, including coarsening. Furthermore, the local atomic arrangement during the whole thermal cycle should be considered in physical modeling to be able to make fully accurate predictions of phase separation in Fe-Cr alloys.

## Acknowledgements

This work was performed within the VINN Excellence Center Hero-m, financed by VINNOVA, the Swedish Governmental Agency for Innovation Systems, Swedish industry and KTH Royal Institute of Technology. X. Xu acknowledges the support from the China Scholarship Council (CSC). We would like to thank the UK Science & Technology Facilities Council for the provision of neutron beam time at ISIS.

## References

[1] I. Cook, Materials research for fusion energy, Nat. Mater. 5 (2006) 77. doi:10.1038/nmat1584.

[2] R.L. Klueh, A.T. Nelson, Ferritic/martensitic steels for next-generation reactors, J Nucl Mater. 371 (2007) 37–52. doi:10.1016/j.jnucmat.2007.05.005.

[3] E.L. Huston, J.W. Cahn, J.E. Hilliard, Spinodal decomposition during continuous cooling, Acta Metall. 14 (1966) 1053–1062. doi:10.1016/0001-6160(66)90193-3.

[4] H.-O. Carmesin, D.W. Heermann, K. Binder, Influence of a continuous quenching procedure on the initial stages of spinodal decomposition, Zeitschrift Für Phys. B Condens. Matter. 65 (1986) 89–102. doi:10.1007/BF01308403.

[5] H. Pollak, U. Karfunkel, J.A. Lodya, N. Mala, Decomposition of an Fe-Cr 38 wt.% chromium stainless steel at 475 °C, Hyperfine Interact. 94 (1994) 2355–2360. doi:10.1007/BF02063788.

[6] C. Lemoine, A. Fnidiki, J. Teillet, M. Hédin, F. Danoix, Mössbauer study of the ferrite

decomposition in unaged duplex stainless steels, Scr. Mater. 39 (1998) 61–66. doi:10.1016/S1359-6462(98)00133-X.

[7] Y.Z. Vintaykin, V.B. Dmitriyev, V.Y. Kolontsov, Effect of prior heat treatment on the rate of separation of iron-chromium solid solutions, Fiz. Met. Metalloved. 27 (1969) 1131–1133. doi:UDC.669.1.620.193.91.

[8] J.C. LaSalle, L.H. Schwartz, Further studies of spinodal decomposition in Fe-Cr, Acta Metall. 34 (1986) 989–1000. doi:10.1016/0001-6160(86)90208-7.

[9] F. Bley, Neutron small-angle scattering study of unmixing in Fe-Cr alloys, Acta Metall. Mater. 40 (1992) 1505–1517. doi:10.1016/0956-7151(92)90094-U.

[10] J. Zhou, J. Odqvist, J. Ågren, A. Ruban, M. Thuvander, W. Xiong, et al., Direct atom probe tomography observations of concentration fluctuations in Fe-Cr solid solution, Scr. Mater. 98 (2015) 13–15. doi:10.1016/j.scriptamat.2014.10.035.

[11] J. Zhou, J. Odqvist, A. Ruban, M. Thuvander, W. Xiong, J. Ågren, et al., Effect of solution treatment on spinodal decomposition during aging of an Fe-46.5 at.% Cr alloy, J. Mater. Sci. 52 (2017) 326–335. doi:10.1007/s10853-016-0333-6.

[12] C. Lemoine, A. Fnidiki, F. Danoix, M. Hédin, J. Teillet, Mössbauer and atom probe studies on the ferrite decomposition in duplex stainless steels caused by the quenching rate, J. Phys. Condens. Matter. 11 (1999) 1105–1114. doi:10.1088/0953-8984/11/4/018.

[13] M. Hedin, J.P. Massoud, F. Danoix, Influence of the Quenching Rate on the Spinodal Decomposition in a Duplex Stainless Steel, Le J. Phys. IV. 6 (1996) C5-235-C5-240. doi:10.1051/jp4:1996538.

[14] I. Mirebeau, M. Hennion, G. Parette, First Measurement of Short-Range-Order Inversion as a Function of Concentration in a Transition Alloy, Phys. Rev. Lett. 53 (1984) 687–690. doi:10.1103/PhysRevLett.53.687.

[15] I. Mirebeau, G. Parette, Neutron study of the short range order inversion in Fe1−xCrx, Phys. Rev. B. 82 (2010) 104203. doi:10.1103/PhysRevB.82.104203.

[16] J.M. Cowley, An approximate theory of order in alloys, Phys. Rev. 77 (1950) 669–675. doi:10.1103/PhysRev.77.669.

[17] M. Hennion, Chemical SRO effects in ferromagnetic Fe alloys in relation to electronic band structure, J. Phys. F Met. Phys. 13 (1983) 2351–2358. doi:10.1088/0305-4608/13/11/017.

[18] P. Olsson, I.A. Abrikosov, L. Vitos, J. Wallenius, Ab initio formation energies of Fe-Cr alloys, J. Nucl. Mater. 321 (2003) 84–90. doi:10.1016/S0022-3115(03)00207-1.

[19] M.Y. Lavrentiev, R. Drautz, D. Nguyen-Manh, T.P.C. Klaver, S.L. Dudarev, Monte Carlo study of thermodynamic properties and clustering in the bcc Fe-Cr system, Phys. Rev. B - Condens. Matter Mater. Phys. 75 (2007) 1–12. doi:10.1103/PhysRevB.75.014208.

[20] P. Erhart, A. Caro, M. Serrano De Caro, B. Sadigh, Short-range order and precipitation in Fe-rich Fe-Cr alloys: Atomistic off-lattice Monte Carlo simulations, Phys. Rev. B - Condens. Matter Mater. Phys. 77 (2008) 1–9. doi:10.1103/PhysRevB.77.134206.

[21] A. V. Ruban, V.I. Razumovskiy, First-principles based thermodynamic model of phase equilibria in bcc Fe-Cr alloys, Phys. Rev. B. 86 (2012) 174111.

doi:10.1103/PhysRevB.86.174111.

[22] J. Zhou, J. Odqvist, L. Höglund, M. Thuvander, T. Barkar, P. Hedström, Initial clustering – a key factor for phase separation kinetics in Fe–Cr-based alloys, Scr. Mater. 75 (2014) 62–65. doi:10.1016/j.scriptamat.2013.11.020.

[23] M.K. Miller, J.M. Hyde, M.G. Hetherington, A. Cerezo, G.D.W. Smith, C.M. Elliott, Spinodal decomposition in Fe-Cr alloys: Experimental study at the atomic level and comparison with computer models—I. Introduction and methodology, Acta Metall. Mater. 43 (1995) 3385–3401. doi:10.1016/0956-7151(95)00040-3.

[24] R.K. Heenan, J. Penfold, S.M. King, SANS at Pulsed Neutron Sources: Present and Future Prospects, J. Appl. Crystallogr. 30 (1997) 1140–1147. doi:10.1107/S0021889897002173.

[25] Https://doi.org/10.5286/SOFTWARE/MANTID, mantidproject. doi:10.5286/SOFTWARE/MANTID.

[26] O. Arnold, J.C. Bilheux, J.M. Borreguero, A. Buts, S.I. Campbell, L. Chapon, et al., Mantid - Data analysis and visualization package for neutron scattering and μ SR experiments, Nucl. Instruments Methods Phys. Res. Sect. A Accel. Spectrometers, Detect. Assoc. Equip. 764 (2014) 156–166. doi:10.1016/j.nima.2014.07.029.

[27] G.D. Wignall, F.S. Bates, Absolute calibration of small-angle neutron scattering data, J. Appl. Crystallogr. 20 (1987) 28–40. doi:10.1107/S0021889887087181.

[28] J.C. LaSalle, Spinodal decomposition in iron-chromium alloys as characterized by samll angle neutron scattering (thesis), Northwestern University, Evanston, Illinois, 1985.

[29] A. Isalgué, M. Anglada, J. Rodríguez-Carvajal, A. De Geyer, Study of the spinodal decomposition of an Fe-28Cr-2Mo-4Ni-Nb alloy by small-angle neutron scattering, J. Mater. Sci. 25 (1990) 4977–4980. doi:10.1007/BF00580116.

[30] M. Hörnqvist, M. Thuvander, a. Steuwer, S. King, J. Odqvist, P. Hedström, Early stages of spinodal decomposition in Fe–Cr resolved by in-situ small-angle neutron scattering, Appl. Phys. Lett. 106 (2015) 61911. doi:10.1063/1.4908250.

[31] G. KOSTORZ, Small-Angle Scattering and Its Applications to Materials Science, in: G. Kostorz (Ed.), Treatise Mater. Sci. Technol. Neutron Scatt., Academic Press, New York, NY, 1979: pp. 227–289. doi:10.1016/B978-0-12-341815-9.50013-6.

[32] D.L. Price, F. Fernandez-Alonso, An Introduction to Neutron Scattering, in: F. Fernandez-Alonso, D.L. Price (Eds.), Exp. Methods Phys. Sci. Neutron Scatt. – Fundam., Elsevier Inc., Amsterdam, 2013: pp. 1–136. doi:10.1016/B978-0-12-398374-9.00001-2.

[33] B. Hammouda, The SANS toolbox, (2016) http://www.ncnr.nist.gov/staff/hammouda/the_SANS_toolbox.

[34] A. Guinier, G. Fournet, Small-Angle Scattering of X-Rays, John Wiley & Sons, Inc., New York, NY, 1955.

[35] S. Novy, P. Pareige, C. Pareige, Atomic scale analysis and phase separation understanding in a thermally aged Fe-20 at.%Cr alloy, J. Nucl. Mater. 384 (2009) 96–102. doi:10.1016/j.jnucmat.2008.10.008.

[36] C. Pareige, M. Roussel, S. Novy, V. Kuksenko, P. Olsson, C. Domain, et al., Kinetic study of phase transformation in a highly concentrated Fe–Cr alloy: Monte Carlo simulation

versus experiments, Acta Mater. 59 (2011) 2404–2411. doi:10.1016/j.actamat.2010.12.038.

[37] W. Xiong, P. Hedström, M. Selleby, J. Odqvist, M. Thuvander, Q. Chen, An improved thermodynamic modeling of the FeCr system down to zero kelvin coupled with key experiments, Calphad Comput. Coupling Phase Diagrams Thermochem. 35 (2011) 355–366. doi:10.1016/j.calphad.2011.05.002.

[38] J.-O. Andersson, B. Sundman, Thermodynamic properties of the Cr-Fe system, Calphad. 11 (1987) 83–92. doi:10.1016/0364-5916(87)90021-6.

[39] S. Katano, M. Iizumi, Decomposition kinetics in iron-chromium alloys, Phys. B+C. 120 (1983) 392–396. doi:10.1016/0378-4363(83)90413-8.

[40] X. Xu, J. Odqvist, M.H. Colliander, M. Thuvander, A. Steuwer, J.E. Westraadt, et al., Structural Characterization of Phase Separation in Fe-Cr: A Current Comparison of Experimental Methods, Metall. Mater. Trans. A. 47 (2016) 5942–5952. doi:10.1007/s11661-016-3800-4.

[41] H.. Cook, Brownian motion in spinodal decomposition, Acta Metall. 18 (1970) 297–306. doi:10.1016/0001-6160(70)90144-6.

[42] Thermo-Calc Software TCFE8 Steels/Fe-alloys database version 8 (accessed 22 December 2016), 2016.

[43] Thermo-Calc Software MOBFE2 SteelsFe-alloys database version 2 (accessed 22 December 2016), 2016.

[44] K. Binder, D. Stauffer, Theory for the slowing down of the relaxation and spinodal decomposition of binary mixtures, Phys. Rev. Lett. 33 (1974) 1006–1009. doi:10.1103/PhysRevLett.33.1006.

[45] J. Marro, A.B. Bortz, M.H. Kalos, J.L. Lebowitz, Time evolution of a quenched binary alloy. II. Computer simulation of a three-dimensional model system, Phys. Rev. B. 12 (1975) 2000–2011. doi:10.1103/PhysRevB.12.2000.

[46] J. Marro, J.L. Lebowitz, M.H. Kalos, Computer Simulation of the Time Evolution of a Quenched Model Alloy in the Nucleation Region, Phys. Rev. Lett. 43 (1979) 282. doi:10.1103/PhysRevLett.43.282.

[47] J.M. Hyde, M.K. Miller, M.G. Hetherington, a. Cerezo, G.D.W. Smith, C.M. Elliott, Spinodal decomposition in Fe-Cr alloys: Experimental study at the atomic level and comparison with computer models-II. Development of domain size and composition amplitude, Acta Metall. Mater. 43 (1995) 3403–3413. doi:10.1016/0956-7151(95)00041-S.

[48] I.M. Lifshitz, V.V. Slyozov, The kinetics of precipitation from supersaturated solid solutions, J. Phys. Chem. Solids. 19 (1961) 35–50. doi:10.1016/0022-3697(61)90054-3.

[49] C. Wagner, Theory of precipitate change by redissolution, Z. Elektrochem. 65 (1961) 581–591.

[50] D.A. Huse, Corrections to late-stage behavior in spinodal decomposition: Lifshitz-Slyozov scaling and Monte Carlo simulations, Phys. Rev. B. 34 (1986) 7845–7850. doi:10.1103/PhysRevB.34.7845.

[51] V.F. Sears, Neutron scattering lengths and cross sections, Neutron News. 3 (1992) 26–37.

doi:10.1080/10448639208218770.

[52] M.B. Cortie, H. Pollak, Embrittlement and aging at 475 °C in an experimental ferritic stainless steel containing 38 wt.% chromium, Mater. Sci. Eng. A. 199 (1995) 153–163. doi:10.1016/0921-5093(94)09731-3.

[53] P. Hedström, F. Huyan, J. Zhou, S. Wessman, M. Thuvander, J. Odqvist, The 475°C embrittlement in Fe-20Cr and Fe-20Cr-X (X=Ni, Cu, Mn) alloys studied by mechanical testing and atom probe tomography, Mater. Sci. Eng. A. 574 (2013) 123–129. doi:10.1016/j.msea.2013.03.016.

[54] M. Nastar, Beyond the Cahn-Hilliard Equation: a Vacancy-Based Kinetic Theory, Solid State Phenom. 172–174 (2011) 321–330. doi:10.4028/www.scientific.net/SSP.172-174.321.

[55] M. Portmann, B. Schönfeld, G. Kostorz, F. Altorfer, J. Kohlbrecher, Evaluation of diffuse neutron scattering at elevated temperatures and local decomposition in Ni-Au, Phys. Rev. B. 68 (2003) 1–4. doi:10.1103/PhysRevB.68.012103.

[56] L. Reinhard, J.L. Robertson, S.C. Moss, G.E. Ice, P. Zschack, C.J. Sparks, Anomalous-x-ray-scattering study of local order in bcc Fe0.53Cr0.47, Phys. Rev. B. 45 (1992) 2662–2676. doi:10.1103/PhysRevB.45.2662.

[57] P.P. Camus, Atom probe analysis of solute clustering above a miscibility gap, Le J. Phys. Colloq. 48 (1987) C6-331-C6-336. doi:10.1051/jphyscol:1987654.